Bioelectrochemistry 131 (2020) 107373

Contents lists available at ScienceDirect

Bioelectrochemistry

journal homepage: www.elsevier.com/locate/bioelechem

Gold nanocubes embedded biocompatible hybrid hydrogels for electrochemical detection of H_2O_2

Pandiaraj Manickam [a,*], Arti Vashist [b], Sekar Madhu [c], Mohanraj Sadasivam [a], Arunkumar Sakthivel [a,d], Ajeet Kaushik [e], Madhavan Nair [b]

[a] Electrodics and Electrocatalysis Division, CSIR-Central Electrochemical Research Institute, Karaikudi 630 003, Tamil Nadu, India
[b] Department of Immunology & Nano-Medicine, Institute of NeuroImmune Pharmacology, Center for Personalized Nanomedicine, Herbert Wertheim College of Medicine, Florida International University, Miami, FL 33199, USA
[c] Department of Nanoscience & Technology, Bharathiar University, Coimbatore 641 046, India
[d] Academy of Scientific and Innovative Research, Ghaziabad 201 002, Uttar Pradesh, India
[e] Department of Natural Sciences, Division of Sciences, Art & Mathematics, Florida Polytechnic University, Lakeland, FL 33805, USA

ARTICLE INFO

Article history:
Received 10 June 2019
Received in revised form 5 September 2019
Accepted 5 September 2019
Available online 07 September 2019

Keywords:
Hydrogels
Biosensors
Biocompatibility
Gold nanocubes
Chitosan
Cytochrome *c*

ABSTRACT

Smart electrochemical biosensors have emerged as a promising alternative analytical diagnostic tool in recent clinical practice. However, improvement in the biocompatibility and electrical conductivity of the biosensor matrix and the immobilization of various bioactive molecules such as enzymes still remain challenging. The present research reports the synthesis of a biocompatible hydrogel network and its integration with gold nanocubes (AuNCs) for developing a novel biosensor with improved functionality. The interpenetrating hydrogel network consist of biopolymers developed using graft *co*-polymerization of β-cyclodextrin (β-CD) and chitosan (CS). The novelty of this work is in integrating the CS-g-β-CD hydrogel network with conductive AuNCs for improving hydrogel conductivity, biosensor sensitivity and use of the material for a biocompatible sensor. The present protocol advances the state of the art for the utilization of biopolymeric hydrogels system in synergy with an enzymatic biosensing protocol for exclusively detecting hydrogen peroxide (H_2O_2). Immobilization of the mitochondrial protein, cytochrome *c* (cyt *c*) into the hydrogel nanocomposite matrix was performed via thiol cross-linking. This organic-inorganic hybrid nanocomposite hydrogel matrix exhibited high biocompatibility (RAW 264.7 and N2a cell lines), improved electrical conductivity to attain high sensitivity (1.2 mA mM^{-1} cm^{-2}) and a low detection limit (15×10^{-9} M) for H_2O_2.

1. Introduction

Cytochrome *c* (cyt *c*) is a redox-active heme protein located in the mitochondrial membrane and participates in electron transfer reactions of the mitochondria [1,2]. The redox behavior of cyt *c* has been studied widely not only for understanding electron transfer dynamics and redox-induced translational changes [3], but also for creating biosensing systems for a wide variety of biochemical entities including reactive oxygen species (ROS) [4–7]. Our group and others have investigated the redox activity of cyt *c* and developed electrochemical cyt *c* biosensing platforms at various nanostructured modified electrode surfaces [1,8–10]. Recently, we have investigated the structural and mechanistic aspects of cyt *c* peroxidase activity through a computational modeling approach [3]. The focus of the present study was to utilize the peroxidase behavior of the immobilized cyt *c* for an electrochemical biosensor that would monitor changes in H_2O_2 levels. H_2O_2 is one of the most stable ROS, can readily penetrate biological membranes, reacts with redox-active molecules, and can cause oxidative protein modification. Monitoring changes in H_2O_2 levels is important as the changes are closely associated with the degradation or formation of other ROS, such as superoxide ($O_2^{\bullet -}$) and hydroxyl radical ($^{\bullet}OH$).

A wide variety of biosensing strategies for detecting H_2O_2 levels, including cyt *c* as bioreceptor, have been reported [6,11,12]. Recently, core-shell nanoparticles formed using zeolitic imidazolate frameworks and reduced graphene oxide have been investigated for monitoring H_2O_2 levels [13]. However, a focus on such biosensors with improved biocompatibility has received little attention. Immobilization of bioreceptor molecules into a matrix that preserves native catalytic properties without compromising structure and conformation while improving sensor biocompatibility is essential for biosensors for biological applications [14–16]. Hydrogels represent a class of soft materials with unique three-dimensional (3D) polymer networks. These 3D cross-linked materials are biocompatible and provide an interface to biosensing systems as a base material [17–21]. Such hydrated gels also create a suitable microenvironment for enzyme immobilization.

* Corresponding author.
E-mail address: pandiaraj@cecri.res.in (P. Manickam).

https://doi.org/10.1016/j.bioelechem.2019.107373
1567-5394/

Hydrogels of CS and its cross-linked derivatives have been explored as a biocompatible immobilization platform for assessing the direct electrochemistry of proteins and for creating sensitive electrochemical detection systems [16,22]. The functionality of these hydrogel scaffolds could be considerably improved if their electrical properties are enhanced. Approaches including the integration of hydrogels with conducting polymers, functionalization with electroactive motifs and incorporation with the nanoelectrical elements have been investigated for improving the electrical conductivity of the hydrogel networks [23–27].

Due to their high electrical and thermal conductivity, metallic nanostructures, together with the other materials, are a suitable candidate for creating an integrated hydrogel platform. When such conductive nanostructures are embedded or entrapped within a polymeric hydrogel network, the conductivity of the matrix can be tuned on the basis of organic-inorganic hybrid nanocomposite theory [23,26,28]. Gold nanoparticles and their composites have emerged as a potential candidate for electrochemical biosensors due to their important role in biofunctionalization and improving biocompatibility [29–31]. Several groups have reported gold nanoparticle based hydrogel systems and demonstrated their use in biomedical applications [32,33]. In our recent review article, the application of gold nanoparticles integrated hydrogel systems for targeted drug delivery are highlighted [34]. Recently, hydrogels of polyethylene glycol (PEG) have been integrated with gold nanoparticles and micropatterned onto the electrode surface for biosensing application [35]. The incorporation of gold nanoparticles increases the conductivity of a hydrogel matrix 5-fold. Enhancement in the specific surface area to capture a large number of biomolecules has been demonstrated by integrating a hydrogel matrix with gold nanoparticles [36]. Gold nanoparticle which are dispersed in a hydrogel matrix can act as dopant and can improve the optomechanical properties of a sensor system [37].

Although efforts have been made to integrate hydrogel networks with different gold nanoarchitecture, so far, integration of a hydrogel network with gold nanocubes (AuNCs) for biosensing has not been reported. Au nanoparticles with cuboidal shape have been actively studied in recent years because of their potential applications in plasmonics, microelectronics and biosensors [38–40]. Compared with gold nanoparticles, AuNCs exhibit strong multiple plasmon resonance and local field enhancement. These properties have been utilized for SERS and for two-photon photoluminescence applications [41]. The vertices and edges present in AuNCs can enhance local electric-field and optoelectronic properties, which facilitates various applications including electron transfer at biomolecules. Although a few reports on hydrogel based H_2O_2 sensors are available, none of have demonstrated the biocompatibility of the immobilization matrix. While the functionality of a hydrogel can be improved by integrating AuNCs, mechanical properties can be improved by grafting other biocompatible polysaccharides such as cyclodextrins (CD). In recognition of these salient features, we report on the fabrication of hydrogel nanocomposites consisting of AuNCs, CS, and CDs. A hybrid interlinked hydrogel network was used to immobilize cyt *c* to fabricate an enzyme-based biosensor for H_2O_2. A further significant aspect was to investigate the biocompatibility of the hydrogel sensor platform. The nanocomposite hydrogel based on the host-guest chemistry resulted in high sensitivity and a low detection limit for the measurement of H_2O_2 with good biocompatibility.

2. Experimental section

2.1. Reagents

Chitosan, β-cyclodextrin (β-CD), cetyltrimethylammonium bromide (CTAB), gold (III) chloride hydrate, ascorbic acid (AA), sodium borohydride ($NaBH_4$), glutaraldehyde, hydrogen peroxide, sodium hydrogen phosphate, disodium hydrogen phosphate, N-(3-Dimethylaminopropyl)-N′-ethylcarbodiimide hydrochloride (EDC), 3-mercaptoproponaic acid (MPA), N-Hydroxysuccinimide (NHS) were purchased from Sigma-Aldrich. Cyt *c* was purchased from Alfa Aesar. All other chemicals were of analytical grade and all solutions were prepared using ultrapure water.

2.2. Instrumentation

UV–vis absorption characteristics were performed using spectrophotometer (Agilent Technologies 8453). X-ray diffraction (XRD) patterns of the AuNCs were analyzed using XPERT-PRO diffractometer ($\lambda = 1.54060$ Å). The morphologies and elemental analysis of the hybrid hydrogel network were carried out using FE-SEM (FEI Quanta-250 FEG) integrated with EDS. FT-IR analysis of the hydrogel material was carried out using FT-IR spectrometer (Bruker Tensor 27, Germany). High-resolution transmission electron microscopic (HR-TEM) images of the AuNCs were recorded using an FEI TECKNAI-F20 Super-Twin instrument operated at 200 kV. Electrochemical experiments were performed using Potentiostat-BAS 100B (Bioanalytical Systems Inc.). Screen-printed carbon electrodes (SPCE) consisting of carbon as working and reference electrodes and Ag/AgCl as a reference electrode (CH Instruments, Inc., USA) was used for fabricating the sensor.

2.3. Synthesis of AuNCs

A seed-mediated growth method was used for synthesizing homogeneous AuNCs [42]. First, the gold seeds were synthesized by adding freshly prepared ice-cold solution of $NaBH_4$ (0.01 M, 0.3 mL) into a solvent mixture composed of CTAB (0.1 M, 3.75 mL) and $HAuCl_4$ (0.01 M,0.125 mL), followed by immediate inversion mixing of the resultant solution for 2 min. The seed solution was kept at room temperature for 60 min to decompose excess borohydride. Growth solution was then prepared by adding CTAB (0.1 M, 3.2 mL), $HAuCl_4$ (0.01 M, 0.4 mL), and ascorbic acid (0.1 M, 1.9 mL) sequentially into the water (16 mL). The seed solution stabilized with CTAB was further diluted with water (5-fold). The diluted seed solution (0.01 mL) was mixed slowly with the growth solution. In the final step, the resultant solution mixture was mixed gently for 10 s and kept at room temperature for overnight.

2.4. CS-g-β-CD hydrogel synthesis

CS-g-β-CD hydrogel networks were synthesized using free radical polymerization. First, a clear solution of CS was obtained by dissolving 0. 5% (*w*/w) of CS in 1% of glacial acetic acid. Subsequently, a 0.5% β-CD crystal clear solution (10 mL) was prepared in double-distilled water and mixed with the CS solution at 1:3 (CS:β-CD) ratio. The grafting mixture was further blended for 1–2 h at 500 rpm speed on a magnetic stirrer. β-CD was included for improving the mechanical characteristics of the CS film. The reaction mixture was then kept aside at room temperature for gelation.

2.5. Biosensor fabrication

The AuNCs were first functionalized with cyt *c* before being introduced into the hydrogel network. In order to conjugate protein molecules, AuNCs were initially functionalized with –COOH moieties using MPA as a cross-linker. The concentration of AuNC solution used for preparing the nanocomposite was 0.19 mM. Attachment of cyt *c* molecules to the MPA modified AuNCs was performed using standard EDC/NHS conjugation chemistry [43]. Briefly, 1 mL MPA/AuNCs solution was incubated with 200 mM EDC and 100 mM NHS solution for 2 h whilst stirring. The mixture was then added to 100 mL cyt *c* solution (12.5 mg/mL in 10 mM of PBS) and magnetically stirred overnight at room temperature to form cyt *c* cross-linked AuNCs. 20 μL of the cyt *c* cross-linked AuNCs were mixed with the hydrogel blend and stirred again for an hour to obtain a homogeneous solution. The nanocomposite-hydrogel blend was then drop cast onto the electrode

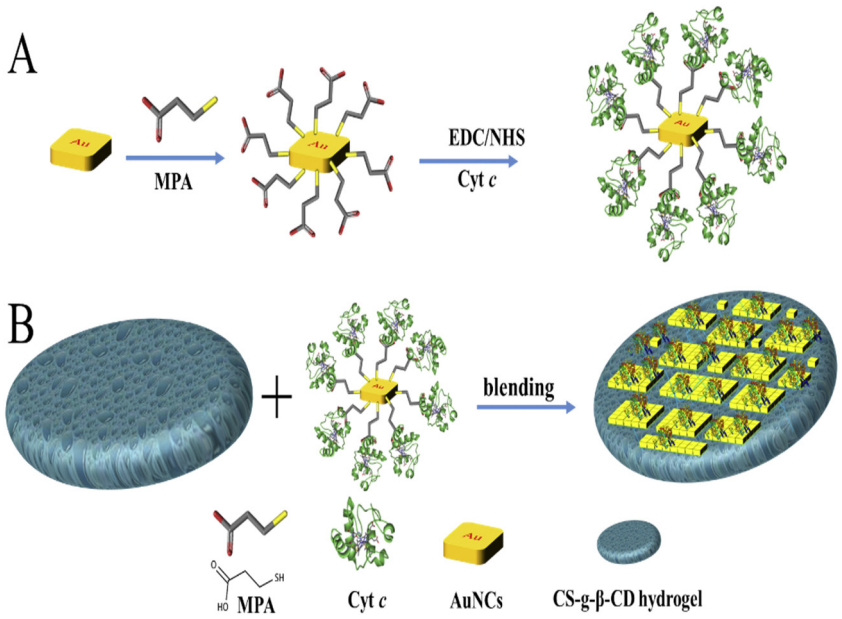

Schematic 1. Steps involved in the fabrication of the AuNCs integrated hydrogel biosensor system: Immobilization of the cyt *c* on AuNCs (A), and integration of the enzyme immobilized AuNCs into the hydrogel network.

surface and used as a biosensor for monitoring H_2O_2 levels. The stepwise fabrication of the biosensor is shown in Schematic 1.

2.6. In vitro cytotoxicity

In order to investigate the biocompatibility of the hybrid hydrogel materials, in vitro cytotoxicity was performed using MTT assay on two different cell lines (RAW 264.7-mouse leukemic monocyte-macrophage cells and N2a-mouse neuroblastoma (N2a) cells). The cell lines were maintained in 75 cm^2 culture flasks in DMEM medium containing 10% streptomycin (100 μg/mL), fetal bovine serum (FBS), and penicillin (100 U/mL) under humidified incubator chamber at 37 °C. Following this, 1.5×10^4 cells/well were seeded in a 96-well plate and allowed to attach for 6 h. Subsequently, the cells were exposed with different concentrations of AuNCs integrated CS-g-β-CD and CS-g-β-CD hydrogels in DMEM lacking FBS for the duration of 24 h. The cells not

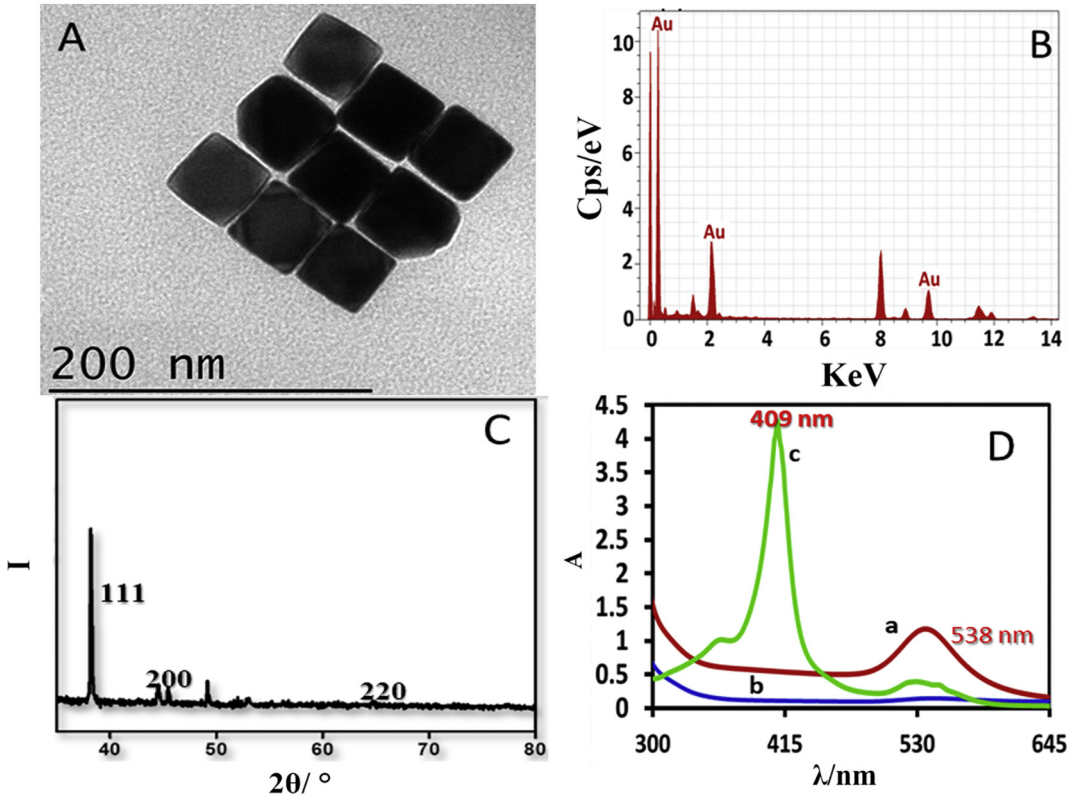

Fig. 1. TEM image (A), EDX spectrum (B), XRD pattern (C) of AuNCs; (D) UV–vis absorption spectra of AuNCs (curve a), MPA/AuNCs (curve b), and cyt *c*/MPA/AuNCs (curve c).

exposed to the hydrogels and exposed to doxorubicin were used as control and positive control, respectively. Following treatment, cell morphologies were examined using an Olympus CKX41 microscope and photographed using Olympus imaging corp. Digital camera (Model E-330). The MTT assay was performed using a reported protocol [35] and the optical density of formazan dissolved in DMSO was determined at 570 nm using a multi-plate reader (Synergy H1, BioTek, USA).

3. Results and discussion

3.1. Structural characterization of AuNCs and conjugation of cyt c

The synthesized AuNCs were characterized using TEM, UV–vis spectroscopy, and XRD. Fig. 1A shows the TEM images of CTAB stabilized AuNCs. The AuNCs structures were uniformly distributed and had a mean edge length of 40.2 nm, with a standard deviation of 5.7 nm. Fig. 1B shows the EDS spectrum recorded for the AuNCs and confirmed the presence of elemental gold. The XRD patterns recorded for the AuNCs are displayed in Fig. 1C. Peaks corresponding to the (111), (200), and (220) planes of a face-centered cubic lattice of gold were observed for AuNCs [44]. The XRD data thus revealed that the gold nanostructure formed is crystalline cubic, as supported by Fig. 1A. Fig. 1D depicts the UV–vis absorption spectra of AuNCs (a), MPA modified AuNCs (b), and cyt *c*/MPA/AuNCs (c). AuNCs exhibited a strong localized surface plasmon resonance (LSPR) at 538 nm [38] (curve a). After modification with MPA (curve b) the absorption peak intensity of the LSPR band associated with the AuNCs decreases. This could be interpreted as MPA assembling and creating a dielectric layer on the AuNCs. When cyt *c* was conjugated with the MPA, new peaks located at 409, 520 and 550 nm (curve c) corresponded to cyt *c*, indicating Soret bands resulting from π-π* transition of the heme-porphyrin ring and confirming enzyme conjugation to AuNCs [45]. These results confirm that cyt *c* was successfully conjugated to the MPA/AuNCs. After modification with MPA and cyt *c*, the diameter of the AuNCs increased to ca. 200–250 nm (Fig. S1). This change in particle size could be attributed to the successful assembly of MPA and cyt *c* molecules onto the AuNCs. The absorption properties of the heme present in native cyt *c* can be used to confirm the conjugation of cyt *c* to AuNCs (Fig. S2).

3.2. Characterization of CS-g-β-CD hydrogel

The prepared CS-g-β-CD hydrogels were characterized using FT-IR, EDS, and FE-SEM. Spatial distribution studies of AuNCs integrated into the hydrogel was also performed using elemental mapping analysis. FE-SEM image reveals a porous morphology in the inter-linked CS-g-β-CD hydrogel network (Fig. 2A). Fig. 2B shows the FT-IR spectra observed for CS, β-CD, and CS-g-β-CD hydrogel. In the FT-IR spectrum of CS, the O—H and N—H stretching bands are overlapped into a broad peak at 3000–3600 cm^{-1}. Bands corresponding to the amide and amine group of CS were observed at 1630 and 1524 cm^{-1}, respectively. The saccharide oxygen bridge peaks of the skeletal vibrations involving the C—O stretching appeared between 1152 and 1090 cm^{-1}. The FT-IR spectrum of β-CD showed that the peaks correspond to the O—H stretching vibration, C—H stretching vibration, C—O stretching vibration, and –OH bending vibration were observed at ~3386 cm^{-1}, 2925 cm^{-1}, 1028 cm^{-1} and 1418 cm^{-1} respectively [22]. The FT-IR spectrum of the CS-g-β-CD hydrogel shows that the C—H stretching vibration peak observed for β-CD (2925 cm^{-1}) disappeared while the C—O stretching band for CS (1152 and 1090 cm^{-1}) decreased after the gel formation. FT-IR results confirmed that the structures of both

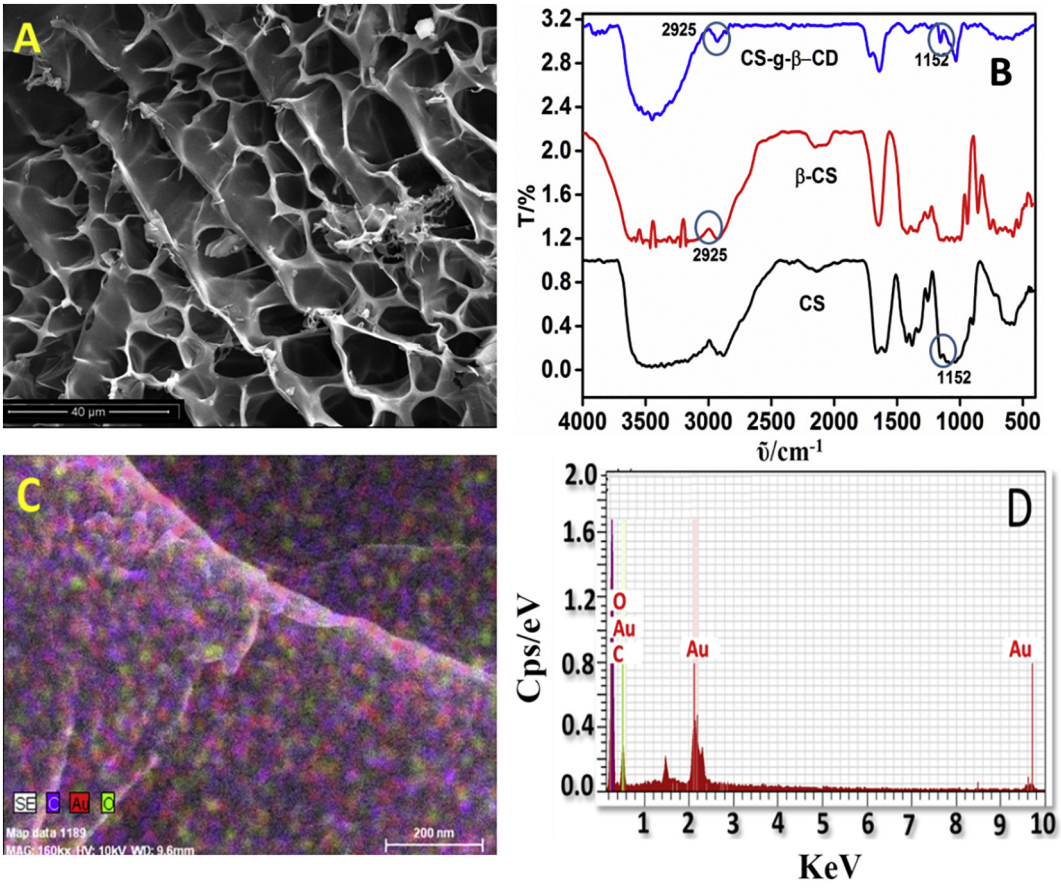

Fig. 2. FE-SEM image of CS-g-β-CD hydrogel (A), FT-IR spectra of CS, β-CD, and CS-g-β-CD hydrogel (B), elemental mapping analysis (C) and EDS spectrum of AuNCs integrated CS-g-β-CDhydrogel (D).

β-CD and CS were altered and that ionic interaction resulted during the preparation of the interpenetrating hydrogel network. The formation of a broad band (O—H) indicated the formation of strong intermolecular and intramolecular H-bonding [46].

As shown in Fig. 2A, the 3D-porous morphology of the interconnected hydrogel network is comprises of pores with diameters ranging from 5 to 20 μm. However, the diameter of the AuNCs conjugated cyt *c* ranged from 200 to 250 nm. During the integration, enzyme-conjugated AuNCs were embedded homogeneously in the hydrogel matrix (incorporated both within the matrix and also attached to the surface of the hydrogel matrix) with high density. EDS elemental analysis (Fig. 2D) confirmed the presence of elemental gold in the hydrogel network and the color differences observed from the mapping analysis (Fig. 2C) further confirmed the homogeneous loading of AuNCs.

3.3. Electrochemical characterization of hybrid hydrogel enzymatic biosensor

To investigate the effect of AuNCs in improving the conductivity of the CS-g-β-CD hydrogel, electrochemical impedance spectroscopy (EIS) measurements were performed in PBS containing 5 mM $K_3[Fe(CN)_6]/K_4[Fe(CN)_6]$ as redox reporter. Fig. 3A compares the Nyquist plot (Z'' vs. Z') observed for the CS-g-β-CD hydrogels with and without the incorporation of AuNCs. The Nyquist plot includes a semicircular portion and a linear portion. The semicircle portion corresponds to electron transfer resistance (R_{ct}) at the electrode surface and can be used to probe interfacial properties of the modified electrode. As seen from the figure, the R_{ct} value decreases when the gels were integrated with the AuNCs (curve b), indicating that the embedded AuNCs increases the electron transfer characteristics of the inter-linked hydrogel network. The R_{ct} values were measured to be 1.4 kΩ for the AuNC incorporated CS-g-β-CD hydrogel and 5.6 kΩ for CS-g-β-CD alone. A 4-fold enhancement in the conductivity of the CS-g-β-CD hydrogel was observed after the inclusion of AuNCs. Overall, the results indicate that incorporating AuNCs enhanced electron transfer characteristics and improved the conductivity of the hydrogel. Immobilization of cyt *c* in the AuNCs/hydrogel network was studied using cyclic voltammetry. Fig. 3B shows typical voltammograms obtained at (a) bare SPCE, (b) CS-g-β-CD hydrogel, and (c) cyt *c*/MPA/AuNCs/CS-g-β-CD modified SPCE in 0.1 M PBS (pH 7.0). A pair of well-defined characteristic reversible redox peaks were obtained for cyt *c* modified electrodes, while only non-Faradaic currents were detected at a bare SPCE and CS-g-β-CD hydrogel modified electrodes, indicating cyt *c* undertakes direct electron transfer reaction in the molecular hydrogel matrix. The electrochemical results complement the results of the optical studies (Fig. 1D) confirming successful immobilization of cyt *c*. The formal redox potential ($E^0 = (E_{p,a} + E_{p,c})/2$) observed for cyt *c* at the MPA/AuNCs/CS-g-β-CD modified electrode was estimated to be 110.5 mV (vs Ag/AgCl), which is comparable to the results obtained in other reported studies [16]. This confirms that the porous inter-linked hydrogel network integrated with AuNCs favored the attachment of cyt *c* and provided native-like micro-environment for covalent immobilization. Cyt *c* based biosensor could be used as an optimized model system for investigating the peroxidase reaction as it can avoid O_2 interferences under a controlled biased voltage. The redox activity of cyt *c* involves a single electron transfer, in which the heme iron is switched between a reduced ferrous (Fe^{2+}) state and an oxidized ferric (Fe^{3+}) state leading to H_2O_2 reduction to water. Electrochemical and optical UV–vis measurements were used to investigate the peroxidase activity of cyt *c*. Dose-dependent oxidation modification of cyt *c* induced by H_2O_2 studied at wavelengths ranging from 300 to 650 nm is shown in Fig. 3C. The UV–vis spectra observed for cyt *c* (curve a) shows two distinct UV absorption peaks at 419 and 545 nm, corroborated as Soret and Q-bands of cyt *c*, respectively (vide supra). The intensity of the absorption peaks decreased sharply when H_2O_2 was added and decreased further when the concentration of H_2O_2 was increased, indicating binding of H_2O_2 and its

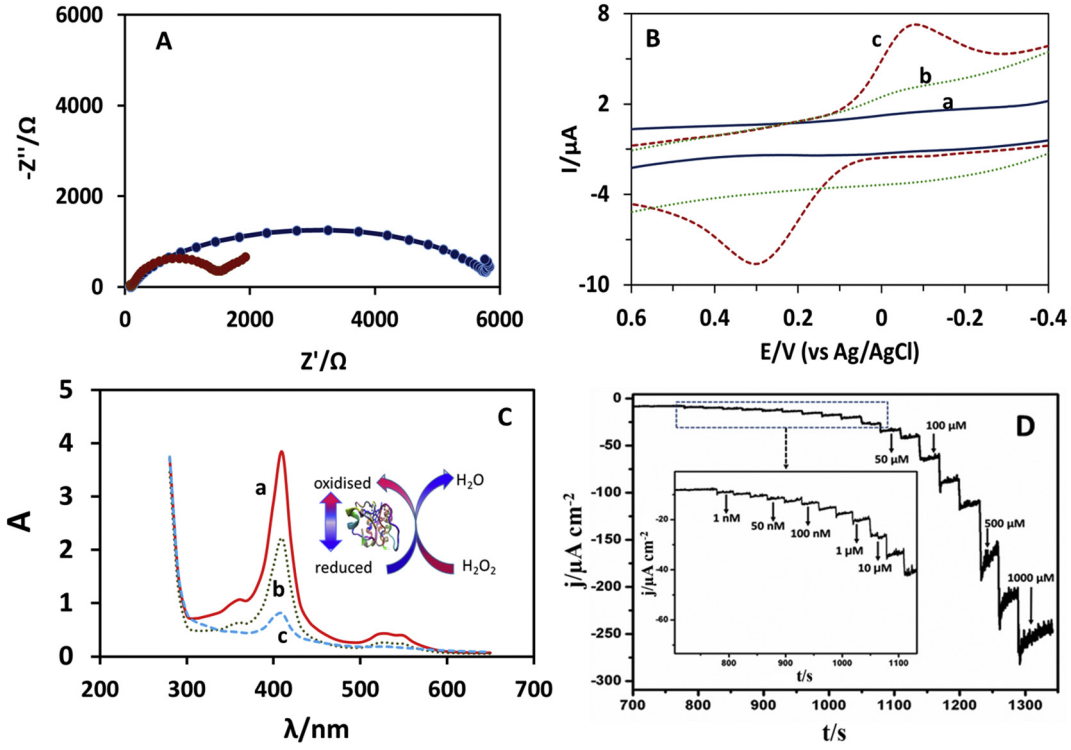

Fig. 3. (A) Electrochemical impedance spectroscopy of hydrogel/AuNCs modified electrodes. Nyquist plots for CS-g-β-CD hydrogels in the presence (b) and absence of (a) of AuNCs. B) Cyclic voltammograms(CVs) obtained for (a) bare SPCE (b) CS-g-β-CD hydrogel/SPCE and (c) cyt *c*/MPA/AuNCs/CS-g-β-CD/SPCE in 0.1 M PBS (pH 7.0) at scan rate of 50 mVs^{-1}. C) Absorption spectra measured for cyt *c* in the presence of different H_2O_2 concentrations (0 mM (a), 0.1 mM (b), and 1 mM (c). D) Amperometric curves obtained for the cyt *c* integrated hydrogel with increase in H_2O_2 concentration from 100 to 1000 μM (inset: amperometric curves obtained for the low H_2O_2 concentrations).

catalytic reaction with cyt *c*. To investigate the electrocatalytic reaction of cyt *c* integrated hydrogel, CV measurements were recorded in 0.1 M PBS (pH 7.0) saturated with oxygen using a scan rate of 50 mVs^{-1} in the presence of various H_2O_2 concentrations. Fig. 3D shows the amperometric curves observed for successive additions of H_2O_2. The amperometric current response changes progressively upon successive addition of H_2O_2, exhibiting a linear range between 0.1 and 1000 μM. The current responses observed for low concentrations of H_2O_2 are shown in Fig. 3D (inset). The calibration curve plotted for the different concentrations of H_2O_2 vs. current is shown in Fig. S3 (inset). Data from Fig. 3D was used for plotting the calibration curve (9 points). Biosensor sensitivity was found to be 18.9 $\mu A\ \mu M^{-1}\ cm^{-2}$. The detection limit was estimated to be 1.5×10^{-9} M at a signal-to-noise ratio of 3.

To evaluate stability, the sensor was stored at 4 °C in 0.1 M PBS after use and tested every day for the current response to 1 mM H_2O_2 for a week. The biosensor retained approximately 80% of its original response over 7 days, indicating excellent stability. Addition of different interference substances such as 1 mM ascorbic acid, citric acid, uric acid, and lactic acid resulted in negligible change (< 2%) in the reduction current, at a negative biasing voltage (−0.15 V). The CV curves obtained for different concentrations of H_2O_2 with the proposed hydrogel-based biosensor are given in fig. S3. A graphic representation of electrochemical reduction reaction occurring at a cyt *c* modified electrode is represented in fig. S3 (inset). Analytical characteristics of the proposed hydrogel-based biosensor, compared with other previously reported H_2O_2 biosensors based on hydrogels is shown in Table S2. Compared to the earlier H_2O_2 biosensors based on hydrogels, the proposed H_2O_2 biosensor, showed a lower detection limit, wider linear range and excellent biocompatibility.

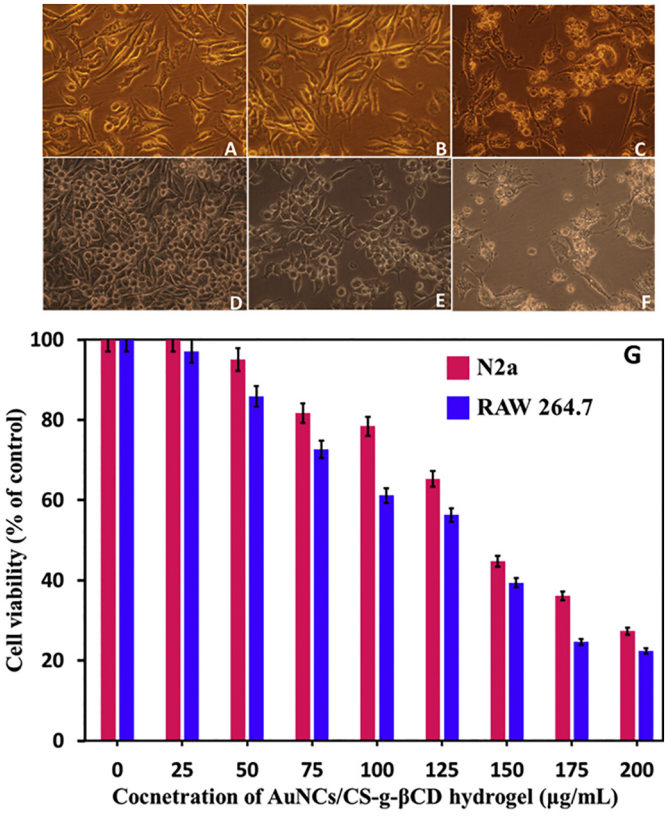

Fig. 4. Morphology of RAW 264.7 and N2a cell lines under fluorescence microscopy. Normal RAW 264.7 cells (A), RAW 264.7 cells treated with 25 μg/mL (B), and IC50 value of AuNCs/CS-g-β-CD hydrogel (127 ± 1.32 μg/mL) (C). Control N2a cells (D), N2a cells treated with 25 μg/mL (E), and IC50 value of AuNCs/CS-g-β-CD hydrogel (110.90 ± 2.52 μg/mL) (F). All images were captured at a magnification of 600×. Cell viability measurement assessed by MTT assay for AuNC incorporated CS-g-β-CD hydrogel.

3.4. Cell viability and in-vitro cytotoxicity analysis

The in-vitro cytotoxicity and cell viability of the synthesized hybrid hydrogel materials (AuNCs/CS-g-β-CD and CS-g-β-CD hydrogel) were investigated using MTT assay. Results indicated that the AuNCs integrated CS-g-β-CD hydrogel at concentrations up to 100 μg/mL, had no significant cytotoxicity for N2a cells (< 20% reduction in cell population) after 24 h of incubation. However, for the RAW 264.7 cells, which appeared to be more sensitive to the hydrogel exposure, cell viability decreased to 65%. When the cells were incubated with AuNCs/CS-g-β-CD hydrogels at concentrations >100 μg/mL, cell viability decreased to almost 50%. However, pristine CS-g-β-CD hydrogel did not show any significant cytotoxic effect up to 1 mg/μL for either cell lines (Table S1). AuNC integrated hydrogel showed higher cytotoxicity compared to their non-AuNCs containing polymer counterparts. This is probably due to the AuNCs. Notably, AuNC integrated hydrogels at high concentration (100 μg/mL) were biocompatible with negligible cytotoxicity and could be utilized as an immobilization platform for biocompatible biosensors. Optical microscopy images were also acquired to directly evaluate the cytotoxicity of the hybrid hydrogel networks (Fig. 4). The optical images of RAW 264.7 and N2a cell lines exposed to different concentration of hydrogels are shown in Fig. 4. After incubation with 25 μg/mL AuNCs/CS-g-β-CD for 24 h, the cell lines retained a similar morphology to control groups. However, at 125 μg/mL, the hydrogel produced notable toxicity to the cells as observed in Fig. 4.

4. Conclusion

In this study, we investigated an AuNC integrated CS-g-β-CD hydrogel network as an advanced biocompatible platform for an enzymatic biosensor. Integration of conducting AuNCs structures within the three-dimensional inter-linked hydrogel network improved electrical conductivity as well as the electron transfer characteristics of the immobilized enzyme for biosensing. Inclusion of AuNCs increased the conductivity of the CS-g-β-CD hydrogel 4 fold. A higher concentration of AuNCs integrated hydrogels (100 μg/mL) were found to be less-cytotoxic to cells (almost 100 times less cytotoxic) than conventional chemotherapeutic drug. As these hybrid hydrogels offer a non-fouling matrix, they have a great potential in eliminating biosensor fouling in complex samples including physiological fluids such as blood or cell culture media.

Acknowledgment

MP acknowledges the funding from CSIR (MLP-0207B). Authors acknowledge respective departments for providing resource and facilities.

Declaration of Competing Interest

Authors declare no conflict of interest.

Appendix A. Supplementary data

Supplementary data to this article can be found online at https://doi.org/10.1016/j.bioelechem.2019.107373.

References

[1] P. Manickam, A. Kaushik, C. Karunakaran, S. Bhansali, Recent advances in cytochrome c biosensing technologies, Biosens. Bioelectron. 87 (2017) 654–668, https://doi.org/10.1016/j.bios.2016.09.013.
[2] C. Garrido, L. Galluzzi, M. Brunet, P.E. Puig, C. Didelot, G. Kroemer, Mechanisms of cytochrome c release from mitochondria, Cell Death Differ. 13 (2006) 1423.
[3] G. Muneeswaran, M. Pandiaraj, S. Kartheeswaran, M. Sankaralingam, K. Muthukumar, C. Karunakaran, Molecular dynamics simulation approach to explore atomistic molecular mechanism of peroxidase activity of apoptotic cytochrome c mutants, Informatics Med. Unlocked. 11 (2018) 51–60.

[4] R.E. Ozel, G. Bulbul, J. Perez, N. Pourmand, Functionalized quartz Nanopipette for intracellular superoxide sensing: A tool for monitoring reactive oxygen species levels in single living cell, ACS Sensors. 3 (2018) 1316–1321.

[5] A.M. Firsov, E.A. Kotova, Y.N. Antonenko, Calcein leakage as a robust assay for cytochrome c/H_2O_2–mediated liposome permeabilization, Anal. Biochem. 552 (2018) 19–23.

[6] Y. Kim, J.Y. Park, H.Y. Kim, M. Lee, J. Yi, I. Choi, A single nanoparticle-based sensor for hydrogen peroxide (H_2O_2) via cytochrome *c*-mediated plasmon resonance energy transfer, Chem. Commun. 51 (2015) 15370–15373.

[7] Y. Luo, H. Liu, Q. Rui, Y. Tian, Detection of extracellular H_2O_2 released from human liver cancer cells based on TiO_2 nanoneedles with enhanced electron transfer of cytochrome *c*, Anal. Chem. 81 (2009) 3035–3041.

[8] M. Pandiaraj, N.K. Sethy, K. Bhargava, V. Kameswararao, C. Karunakaran, Designing label-free electrochemical immunosensors for cytochrome *c* using nanocomposites functionalized screen printed electrodes, Biosens. Bioelectron. 54 (2014) 115–121.

[9] M. Pandiaraj, T. Madasamy, P.N. Gollavilli, M. Balamurugan, S. Kotamraju, V.K. Rao, K. Bhargava, C. Karunakaran, Nanomaterial-based electrochemical biosensors for cytochrome c using cytochrome c reductase, Bioelectrochemistry. 91 (2013) 1–7, https://doi.org/10.1016/j.bioelechem.2012.09.004.

[10] T. Madasamy, C. Santschi, O.J.F. Martin, A miniaturized electrochemical assay for homocysteine using screen-printed electrodes with cytochrome c anchored gold nanoparticles, Analyst. 140 (2015) 6071–6078.

[11] B. Dinesh, V. Mani, R. Saraswathi, S.-M. Chen, Direct electrochemistry of cytochrome c immobilized on a graphene oxide–carbon nanotube composite for picomolar detection of hydrogen peroxide, RSC Adv. 4 (2014) 28229–28237.

[12] Q. Rui, K. Komori, Y. Tian, H. Liu, Y. Luo, Y. Sakai, Electrochemical biosensor for the detection of H2O2 from living cancer cells based on ZnO nanosheets, Anal. Chim. Acta 670 (2010) 57–62.

[13] Z. Li, Y. Jiang, Z. Wang, W. Wang, Y. Yuan, X. Wu, X. Liu, M. Li, S. Dilpazir, G. Zhang, Nitrogen-rich core-shell structured particles consisting of carbonized zeolitic imidazolate frameworks and reduced graphene oxide for amperometric determination of hydrogen peroxide, Microchim. Acta 185 (2018) 501.

[14] L. Zhang, Y. Tian, Designing recognition molecules and tailoring functional surfaces for in vivo monitoring of small molecules in the brain, Acc. Chem. Res. 51 (2018) 688–696.

[15] G. Justin, S. Finley, A.R. Abdur Rahman, A. Guiseppi-Elie, Biomimetic hydrogels for biosensor implant biocompatibility: electrochemical characterization using microdisc electrode arrays (MDEAs), Biomed. Microdevices 11 (2009) 103–115, https://doi.org/10.1007/s10544-008-9214-3.

[16] J. Zhou, C. Liao, L. Zhang, Q. Wang, Y. Tian, Molecular hydrogel-stabilized enzyme with facilitated electron transfer for determination of H_2O_2 released from live cells, Anal. Chem. 86 (2014) 4395–4401.

[17] M.B. Nagarajan, A.M. Tentori, W.C. Zhang, F.J. Slack, P.S. Doyle, Nonfouling, encoded hydrogel microparticles for multiplex MicroRNA profiling directly from formalin-fixed, paraffin-embedded tissue, Anal. Chem. 90 (2018) 10279–10285.

[18] G.C. Le Goff, R.L. Srinivas, W.A. Hill, P.S. Doyle, Hydrogel microparticles for biosensing, Eur. Polym. J. 72 (2015) 386–412.

[19] A. Vashist, A. Kaushik, A. Vashist, V. Sagar, A. Ghosal, Y.K. Gupta, S. Ahmad, M. Nair, Advances in carbon nanotubes–hydrogel hybrids in nanomedicine for therapeutics, Adv. Healthc. Mater. 7 (2018), 1701213.

[20] R. Kouser, A. Vashist, M. Zafaryab, M.A. Rizvi, S. Ahmad, Biocompatible and mechanically robust nanocomposite hydrogels for potential applications in tissue engineering, Mater. Sci. Eng. C 84 (2018) 168–179.

[21] I.Y. Jung, J.S. Kim, B.R. Choi, K. Lee, H. Lee, Hydrogel based biosensors for in vitro diagnostics of biochemicals, proteins, and genes, Adv. Healthc. Mater. 6 (2017), 1601475.

[22] H.Y. Zhou, Z.Y. Wang, X.Y. Duan, L.J. Jiang, P.P. Cao, J.X. Li, J.B. Li, Design and evaluation of chitosan-β-cyclodextrin based thermosensitive hydrogel, Biochem. Eng. J. 111 (2016) 100–107.

[23] L. Li, Y. Wang, L. Pan, Y. Shi, W. Cheng, Y. Shi, G. Yu, A nanostructured conductive hydrogels-based biosensor platform for human metabolite detection, Nano Lett. 15 (2015) 1146–1151.

[24] M. Kim, J.E. Kwon, K. Lee, W.-G. Koh, Signal-amplifying nanoparticle/hydrogel hybrid microarray biosensor for metal-enhanced fluorescence detection of organophosphorus compounds, Biofabrication. 10 (2018), 35002.

[25] L. Li, L. Pan, Z. Ma, K. Yan, W. Cheng, Y. Shi, G. Yu, All inkjet-printed amperometric multiplexed biosensors based on nanostructured conductive hydrogel electrodes, Nano Lett. 18 (2018) 3322–3327.

[26] D. Zhai, B. Liu, Y. Shi, L. Pan, Y. Wang, W. Li, R. Zhang, G. Yu, Highly sensitive glucose sensor based on Pt nanoparticle/polyaniline hydrogel heterostructures, ACS Nano 7 (2013) 3540–3546.

[27] V.A. Pedrosa, J. Yan, A.L. Simonian, A. Revzin, Micropatterned nanocomposite hydrogels for biosensing applications, Electroanalysis. 23 (2011) 1142–1149, https://doi.org/10.1002/elan.201000654.

[28] S.K. Krishnan, E. Prokhorov, D. Bahena, R. Esparza, M. Meyyappan, Chitosan-covered Pd@ Pt Core–Shell Nanocubes for direct Electron transfer in electrochemical enzymatic glucose biosensor, ACS Omega. 2 (2017) 1896–1904.

[29] H.-L. Shuai, X. Wu, K.-J. Huang, Z.-B. Zhai, Ultrasensitive electrochemical biosensing platform based on spherical silicon dioxide/molybdenum selenide nanohybrids and triggered hybridization chain reaction, Biosens. Bioelectron. 94 (2017) 616–625.

[30] Y.-H. Wang, K.-J. Huang, X. Wu, Y.-Y. Ma, D.-L. Song, C.-Y. Du, S.-H. Chang, Ultrasensitive supersandwich-type biosensor for enzyme-free amplified microRNA detection based on N-doped graphene/Au nanoparticles and hemin/G-quadruplexes, J. Mater. Chem. B 6 (2018) 2134–2142.

[31] Y.-H. Wang, H. Xia, K.-J. Huang, X. Wu, Y.-Y. Ma, R. Deng, Y.-F. Lu, Z.-W. Han, Ultrasensitive determination of thrombin by using an electrode modified with WSe_2 and gold nanoparticles, aptamer-thrombin-aptamer sandwiching, redox cycling, and signal enhancement by alkaline phosphatase, Microchim. Acta 185 (2018) 502.

[32] D. Lee, D.N. Heo, H.R. Nah, S.J. Lee, W.-K. Ko, J.S. Lee, H.-J. Moon, J.B. Bang, Y.-S. Hwang, R.L. Reis, Injectable hydrogel composite containing modified gold nanoparticles: implication in bone tissue regeneration, Int. J. Nanomedicine 13 (2018) 7019.

[33] E. Marsich, A. Travan, I. Donati, A. Di Luca, M. Benincasa, M. Crosera, S. Paoletti, Biological response of hydrogels embedding gold nanoparticles, Colloids Surf. B: Biointerfaces 83 (2011) 331–339.

[34] A. Vashist, A. Kaushik, A. Ghosal, J. Bala, R. Nikkhah-Moshaie, W. A Wani, P. Manickam, M. Nair, Nanocomposite hydrogels: advances in nanofillers used for nanomedicine, Gels. 4 (2018) 75.

[35] V.A. Pedrosa, J. Yan, A.L. Simonian, A. Revzin, Micropatterned nanocomposite hydrogels for biosensing applications, Electroanalysis. 23 (2011) 1142–1149.

[36] Q. Rong, H. Han, F. Feng, Z. Ma, Network nanostructured polypyrrole hydrogel/au composites as enhanced electrochemical biosensing platform, Sci. Rep. 5 (2015), 11440.

[37] J. Wang, S. Banerji, N. Menegazzo, W. Peng, Q. Zou, K.S. Booksh, Glucose detection with surface plasmon resonance spectroscopy and molecularly imprinted hydrogel coatings, Talanta. 86 (2011) 133–141.

[38] M. Sundarapandi, P. Viswanathan, S. Sivakumar, R. Ramaraj, Catalytic activities of mono-and bi-metal (gold/silver) nanoshells coated gold nanocubes towards catalytic reduction of nitroaromatics, Langmuir. 34 (2018) 13897–13904.

[39] L. Zhang, J. Wang, J. Zhang, Y. Liu, L. Wu, J. Shen, Y. Zhang, Y. Hu, Q. Fan, W. Huang, Individual Au-Nanocube based Plasmonic Nanoprobe for Cancer relevant MicroRNA biomarker detection, ACS Sensors. 2 (2017) 1435–1440.

[40] J.C. Claussen, A.D. Franklin, A. ul Haque, D.M. Porterfield, T.S. Fisher, Electrochemical biosensor of nanocube-augmented carbon nanotube networks, ACS Nano 3 (2009) 37–44.

[41] Z. Guan, S. Li, P.B.S. Cheng, N. Zhou, N. Gao, Q.-H. Xu, Band-selective coupling-induced enhancement of two-photon photoluminescence in gold nanocubes and its application as turn-on fluorescent probes for cysteine and glutathione, ACS Appl. Mater. Interfaces 4 (2012) 5711–5716.

[42] L. Deng, L. Liu, C. Zhu, D. Li, S. Dong, Hybrid gold nanocube@ silica@ graphene-quantum-dot superstructures: synthesis and specific cell surface protein imaging applications, Chem. Commun. 49 (2013) 2503–2505.

[43] R.E. Ducker, M.T. Montague, G.J. Leggett, A comparative investigation of methods for protein immobilization on self-assembled monolayers using glutaraldehyde, carbodiimide, and anhydride reagents, Biointerphases. 3 (2008) 59–65.

[44] C.-J. Huang, Y.-H. Wang, P.-H. Chiu, M.-C. Shih, T.-H. Meen, Electrochemical synthesis of gold nanocubes, Mater. Lett. 60 (2006) 1896–1900.

[45] M. Collinson, E.F. Bowden, UV-visible spectroscopy of adsorbed cytochrome c on tin oxide electrodes, Anal. Chem. 64 (1992) 1470–1476.

[46] L.D. Wilson, D.Y. Pratt, J.A. Kozinski, Preparation and sorption studies of β-cyclodextrin–chitosan–glutaraldehyde terpolymers, J. Colloid Interface Sci. 393 (2013) 271–277.